Short-range order in crystalline, amorphous, liquid, and supercooled germanium probed by x-ray-absorption spectroscopy

A. Filipponi
Dipartimento di Fisica, Università degli Studi dell' Aquila, via Vetoio, 67010 Coppito, L' Aquila, Italy

A. Di Cicco
Dipartimento di Matematica e Fisica, Università di Camerino, via Madonna delle Carceri, 62032 Camerino (MC), Italy

(Received 26 September 1994; revised manuscript received 15 December 1994)

A detailed experimental investigation of the short-range structural properties in condensed phases of germanium is presented. X-ray-absorption measurements at the Ge K edge have been collected in a wide temperature range for different samples. Polycrystalline c-Ge was measured at 77, 296, 450, 620, 782, 920, and at 1100 K, close to the Ge melting-point temperature $T_m = 1210.4$ K. Evaporated amorphous Ge was measured at 297 K. Eight independent measurements for liquid germanium have been collected from about 950 K in highly supercooled conditions up to about 1600 K. The spectra show a remarkable temperature trend. By comparison, previous diffraction measurements on l-Ge were limited to two narrow temperature regions only, either above T_m or around 1500 K, and no measurements in the supercooled liquid region existed. Data analysis has been performed with the GNXAS approach and account has been taken for the presence of double-excitation channels involving $3d$ and $3p$ electrons in addition to the $1s$. The c-Ge structural results are found in excellent agreement with the known properties. The expansion of the average bond length R is in agreement with thermal expansion data. Mean-square vibrational amplitudes are in excellent agreement with both previous measurements and calculations in the harmonic approximation. The analysis of the signal in liquid Ge has been performed using a technique that allows to extract information on the radial distribution function $g(r)$ directly comparable with molecular dynamics (MD) simulations or previous diffraction determinations. A regular trend is observed in the intensity of the first $g(r)$ peak that decreases from 2.3 at 950 K to about 1.8 at 1610 K. At the same time a widening of the peak and a shift of the rising short distance edge is clearly detected. The data are in excellent agreement with diffraction measurements and recent *ab initio* MD results by Kresse and Hafner [Phys. Rev. B **49**, 14 251 (1994)]. The general relevance of these findings, in connection with the possibility to obtain structural information for liquid systems complementary to that contained in diffraction measurements, is addressed.

I. INTRODUCTION

Structural investigations on condensed phases of Ge are of fundamental interest due to the interplay between the covalent and metallic characters of the bonding. Research in this field is also relevant to several applied physics problems and semiconductor technology.

Ge manifests a large degree of polymorphism in its solid phases. The stable crystalline phase at ambient pressure is the diamond structure where each Ge atom is surrounded by four covalently bonded first neighbors in a tetrahedral symmetry. This form of Ge is semiconducting with an indirect gap of about 0.7 eV. The diamond structure has a very low density with respect to close packing. Upon application of pressure the tetrahedral bonding network is broken and the number of neighbors and the density increase. Around 100 kbar a phase transition to the metallic β-Sn structure[1] occurs, and at even higher pressures an hexagonal phase and a close-packed phase are produced.[2] On releasing the pressure from the β-Sn phase two semiconducting metastable phases denominated ST12 (Ref. 3) and BC8 (Ref. 4) are sometimes observed. These phases are denser than the diamond structure still preserving fourfold coordination; they have been the subject of several recent experimental[5] and theoretical[6] works.

At standard pressure the melting-point temperature for c-Ge is $T_m = 1210.4$ K, a value that decreases on increasing pressure.[7] At the melting transition the tetrahedral network is also broken, and a semiconductor–liquid-metal transition occurs. The electrical resistivity decreases by a factor of about 11 and, at the same time, the density increases by about 5%,[8] while the average coordination number increases from 4 to about 7.

Molten germanium (l-Ge) can be supercooled to a high degree;[9,10] however, it cannot be quenched in the glassy state even with the fastest cooling rates obtainable under laboratory conditions. On the other hand, solid germanium can be directly deposited in an amorphous form by evaporation or sputtering techniques.[11] Amorphous ger-

manium (a-Ge) is an amorphous semiconductor made of a continuous random network of slightly distorted tetrahedral units[11] with a certain percentage of defects. Differences in the fine structural details have been found depending on the deposition method and parameters. If the a-Ge films are heated above about 200 °C, they start to crystallize around nucleation centers.

A very similar phenomenology for what concerns the solid polymorphism, liquid metallic phase, and amorphous structure, is observed for silicon.

The theoretical understanding of the complex interplay between covalent and metallic bonding character has been the subject of several investigations.[12,13] Molecular dynamics (MD) simulations of l-Ge (and l-Si) have been performed using several schemes including empirical (Stillinger-Weber) potentials,[14] pair interactions derived from the pseudopotential theory,[15] and *ab initio* MD schemes.[16,17] The role of the complex electronic interaction has been largely emphasized. Calculated pair correlation properties for the liquid phase are usually found to be in reasonable agreement with the experiments and differ only slightly between different computational schemes. However, an accurate description of the interplay between metallic and covalent characters in molten germanium or silicon can only be provided by *ab initio* MD simulations. The Car-Parrinello method[16] was first used to perform an *ab initio* MD simulation on l-Si.[18] An improved *ab initio* MD scheme[19] has been recently used to simulate condensed phases of Ge, and a deep insight into the structural and electronic problems was provided.[20] Another recent *ab initio* MD simulation at 1500 K was performed using the Car-Parrinello method.[21]

Several experiments on liquid Ge have been performed with either x-ray;[22–24] or neutron-diffraction (ND) techniques[25–28] and various detection methods. An updated list of the available measurements was recently reported.[24] The measurements are concentrated in two temperatures regions: just above the melting point and around 1500 K. From the measurements available in an extended k range radial distribution functions $g(r)$ have been derived. An expanded plot of the $g(r)$'s determined in various diffraction experiments is reproduced in Fig. 1. There is a certain spread in the available data especially for what concerns the peak intensity, indicating in some cases the existence of significant experimental uncertainties. Open questions are the establishment of the present accuracy of the diffraction measurements, also in connection with the comparison between neutron and x-ray results.[28]

In this context the role of an alternative structural technique can be large. Recent advances in the theory and interpretation of the extended x-ray absorption fine structure (EXAFS) and the development of the GNXAS [acronym composed of g_n, n-body distribution functions and XAS (x-ray-absorption spectroscopy)] method for data analysis[29–31] have shown that XAS can be a powerful local structural probe, also for liquid systems, and that it can nicely complement the $S(k)$ information.[32] The EXAFS signal is known to be sensitive to local triplet

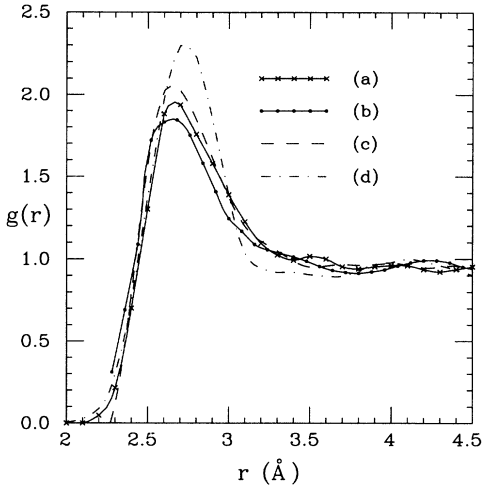

FIG. 1. Comparison among various determinations of the $g(r)$ of liquid germanium in the 940–1000 °C temperature range. Curve (a) (Ref. 24, XRD), curve (b) (Ref. 25, ND), curve (c) (Ref. 28, ND), and curve (d) (Ref. 23, XRD). Only the detail of the first-peak region is shown; remarkable differences are found.

correlations through the presence of strong multiple-scattering (MS) effects. The GNXAS data-analysis methodology proved capable to derive quantitative information on the three-body correlations in molecular and crystalline,[31] but also amorphous[33] and liquid systems. Recent successful applications in different contexts regarded liquid and supercooled Ga (Refs. 34,35) and the hydration shell of aquaions.[36]

One of the most interesting characteristics of XAS in the study of liquid systems is that exactly the same experiment and data analysis can be performed on the same sample in liquid and crystalline phases. The interpretation of the EXAFS of Ge samples can yield an excellent determination of the Ge-Ge first-neighbor peak profile in the solid, as a function of temperature, as well as in the liquid. The availability of the c-Ge measurements allows one to calibrate the distance scale to a high degree of accuracy and potentially to obtain a high precision in the distance determination.

Crystalline and amorphous germanium have been widely investigated by EXAFS. Pioneering EXAFS investigations have been performed on c-Ge and a-Ge.[37] Crozier and Seary studied c-Ge up to 1085 K and found only a slight asymmetry of the first-shell peak profile at high temperature.[38] Several papers were devoted to study the ordering preceding crystallization in a-Ge, either annealed or deposited at different substrate temperatures.[39,40] Measurements of a-Ge have been also performed under high-pressure conditions.[41] Another group performed accurate measurements in the 77–400 K range[42] and determined the structural parameters for the first three shells in the cumulant expansion formalism.[43] All these previous measurements have either been performed at relatively low temperature or the analysis was limited to the first-shell signal. An EXAFS measurement of liquid Ge was previously reported,[44] but very little insight was provided.

Further progress was recently made in the experimental setups for high-temperature x-ray absorption measurements. A design for high-temperature oven and a sample preparation technique suitable to reach temperatures in the 3000 K range[45] were developed by us. These methodologies proved to be suitable to study several liquid systems and in particular solid and liquid Ge at high temperatures.

With the present experimental setup and the advanced GNXAS data-analysis method, we started a wide research project to determine the short-range structural properties of condensed phases of Ge, as seen by EXAFS. This includes (a) an improved analysis of the c-Ge spectrum up to the third shell possibly accounting for MS effects, from 77 K up to the melting point; (b) the measurement and the structural analysis of the liquid Ge EXAFS spectra, as a function of temperature, ranging from highly supercooled conditions (that cannot be reached by diffraction experiments) to the evaporation threshold; and (c) the understanding of the short-range structural properties in the various phases and the comparison with previous diffraction measurements and simulations. This project is widely justified by the interest in the systems being investigated and by the improvements with respect to previous studies.

In the present paper we will present most of the experimental results and a complete analysis of the short-range structural properties in c-Ge, a-Ge, l-Ge, and supercooled l-Ge. The interpretation of the signal beyond the pair correlation properties has been addressed elsewhere.[46]

The paper is organized as follows. Section II contains details on the sample preparation technique and XAS measurements, Sec. III contains the description of the data-analysis methods and the results divided into c-Ge (a-Ge) and l-Ge spectra, and finally concluding remarks are reported in Sec. IV.

II. EXPERIMENTAL DETAILS

A. Sample preparation

The c-Ge samples were prepared starting from commercial c-Ge (99.99% purity) powder. The powder was finely ground in a mortar, suspended in CH_3OH, and poured into a cylinder. The suspension was allowed to settle for several hours and only the smallest particles filtered through a polycarbonate membrane. Electron microscope photographs of the powder reveals c-Ge crystallites with an average size around 0.2–0.4 μm. Notice that this is still large enough to probe bulk properties with a transmission experiment. Weighted amounts of this finely ground powder and of an inert matrix powder (in this case either BN or graphite powders were used), typically in a weight ratio 1:10-1:20, were then mixed in a CH_3OH suspension and finely dispersed using an ultrasonic bath. In this way an homogeneous mixture of isolated Ge and matrix particles was obtained. The mixture was then filtered through a polycarbonate membrane and dried. Finally it was pressed into a pellet of a typical thickness of 0.5–1 mm. This sample preparation procedure guarantees that the sample is not affected by Ge thickness inhomogeneities. The optimal sample thickness for absorption measurements at the Ge K edge is about 11 μm and therefore in order to avoid well-known nonlinear effects in the absorption detection[47–49] the powdered starting material has to be very fine ($\leq$ 1 μm in size) and also homogeneously dispersed in the matrix material (there is no advantage in operating a fine fragmentation if the powder coalesces in larger grains in the final mixture).

Powdered c-Ge samples can be affected by oxygen contamination. Even for a 1 μm cubic particle with a surface oxide layer of 100 Å a macroscopic volume fraction $\approx 6/100$, which is observable with x-ray-absorption techniques, would result in being contaminated. The contamination effect is reduced if the particle size is increased, but then nonlinear problems in the absorption detection are likely to be present.

Our strategy has been to purify the sample *in situ*, following well-established procedures.[50] It is well known that GeO_2 can be easily reduced to Ge, and also that GeO is an extremely volatile specimen at temperatures above 710 °C. When Ge is heated in vacuum, close to or above T_m, the oxidized part evaporates and the material left in the sample container is progressively reduced. The purification of the sample can be further verified *in situ* with an EXAFS experiment and checked following successive melting and recrystallization cycles. This will be described in detail below.

The a-Ge sample with a total thickness of about 10 μm has been evaporated from commercial Ge 99.999% lumps on a BN substrate. The substrate temperature during the deposition was below the threshold for depositing a microcrystalline specimen.[39]

B. Beam lines and oven

The experiment was performed during several dedicated runs at LURE (Orsay, France) at the D42 (EXAFS 1) beam line, equipped with a Si (331) channel-cut monochromator. Preliminary measurements were also obtained at the D44 beam line equipped with a double-crystal Si (311) monochromator. The DCI storage ring was operating at 1.85 GeV with typical currents of about 300 mA.

The high-temperature x-ray-absorption measurements have been performed with a recently developed high-temperature oven.[45] The oven operates in vacuum and the sample is placed in an electrically heated crucible made of a folded graphite sheet. The temperature in this case was controlled by a Chromel-Alumel thermocouple placed directly in contact with the sample, through the crucible. The homogeneity of the temperature within the sample area can be estimated, from finite element thermal analysis,[45] to be within 5 °C. Errors quoted in the measured temperatures, indicated in the tables reported below, include the effects of temperature gradients induced by the nonideal crucible geometries. An independent temperature check was also given by the Ge melting point.

The 77 K spectra have been recorded using the standard liquid-nitrogen beam line cryostat.

C. *In situ* purification

Typical K-edge spectra recorded during the *in situ* purification phase of the c-Ge sample are shown in Fig. 2. Spectrum (a) refers to an heavily oxidized powder at room temperature (RT), as the temperature is raised to 1180 K, spectrum (b), and above (next spectra) the reduction of the GeO_2 contamination takes place. Simultaneously GeO evaporation produces a progressive decrease of the absorption jump. Eventually the shape of the spectrum stabilizes, and this guarantees that only pure Ge droplets with a very low vapor pressure are left in the sample. This procedure was effective for all Ge samples in both BN or graphite matrices. The purity of the samples was further checked performing successive melting and freezing cycles as described below.

D. Melting-crystallization cycles

The check on the purity of the sample is directly evidenced by the EXAFS analysis; however, a very sensitive test is also provided by the monitoring of the sharpness of the melting transition that can be observed by EXAFS.

When the temperature is raised above T_m the Ge crystallites melt and the sample becomes a dispersion of micrometric Ge droplets into the inert matrix. The surface adhesion between Ge droplets and matrix powder is sufficient to avoid any dispersion of the liquid. The samples can also be heated well above T_m without any appreciable vaporization of the specimen.

When the temperature is lowered below T_m, due to the droplet nature of the sample, crystallization may not take place immediately and a supercooled liquid can be obtained. The supercooling phenomena for liquid droplet samples are well known.[51] Supercooling rates up to $415° \pm 20°$ below T_m were previously observed[9] in Ge droplets.

The absorption coefficient in the Ge K-edge region recorded in several spectra cycling the temperature below and above T_m is shown in Fig. 3. The switching between two typical patterns for c-Ge and l-Ge is clearly visible. The large spectral differences are associated with the onset of the metallic properties. The main peak at the edge increases in intensity and the threshold shifts to lower energy values by about 0.8 ± 0.2 eV. This is clearly related to the disappearance of the gap in the semiconductor-to-metal transition. Similar results have been obtained in a near-edge experiment performed with dispersive EXAFS equipment.[52]

The experiment reported in Fig. 3 was performed on a sample in a graphite matrix. The sequence of the spectra shows the fine reproducibility of the melting and recrystallization phenomena. In particular a sharp melting is repeatedly observed at T_m, within experimental uncer-

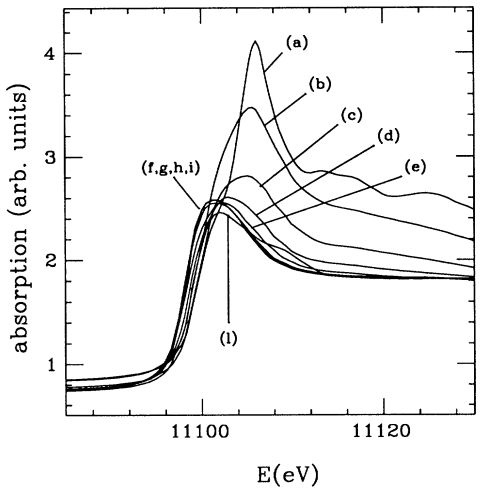

FIG. 2. Successive Ge K-edge spectra recorded during the *in situ* purification of the Ge powder specimen. The approximate temperature in K for the various spectra is (a) 299, (b) 1080, (c) 1240, (d) 1280, (e), (f), (g), (h), (i) 1300, and (l) 1080 with the sample recrystallized. The disappearance of the sharp GeO_2 white line and the threshold shift towards lower energies are a direct evidence for the progressive reduction of the Ge sample. The jump reduction is associated with the evaporation of the volatile oxides.

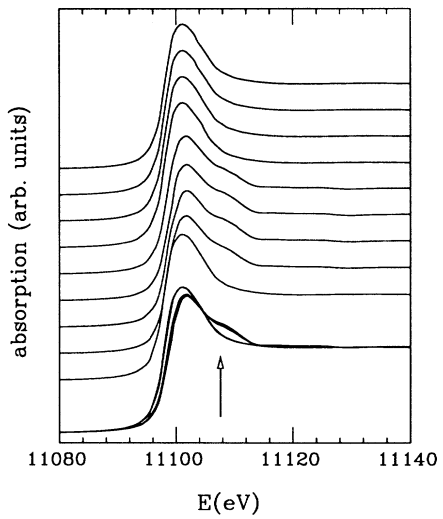

FIG. 3. Ge K-edge x-ray absorption near-edge structure (XANES) of the purified sample in graphite matrix cycled around the melting transition. The nominal temperatures of the successive spectra in K are (from top to bottom) 1234, 1209, 1184, 1159, 1134 (crystallization took place), 1110, 1159, 1184, and 1209 (melting observed). In the bottom curve all the spectra are overlapped to show the switching from two well-defined shapes for the crystalline and liquid specimens, respectively. The melting occurs within 10 °C from the known melting point, that is, within experimental errors. This indicates both sample purity and accuracy in the temperature measurements. Supercooling of about 50 K can be reached with this sample.

tainties. Instead the recrystallization occurs systematically about 50 K below T_m, demonstrating the possibility to produce supercooled liquid Ge samples. The experiment shown in Fig. 3 can be performed after hours of measurements on the liquid sample, indicating that there is no progressive contamination in our experimental setup.

The melting-crystallization experiment was performed in an identical way with the BN matrix samples. In this case an exceptional supercooling effect was observed, and recrystallization was found to occur only when the sample temperature was lowered below 900 K. A macroscopic percentage of the sample droplets was observed to gradually recrystallize during 20 min of observation at 910 K.

Therefore a remarkably different behavior has been observed between Ge droplets in BN and graphite matrices. For the samples in the graphite matrix a supercooling of only about 50 K could be achieved, and the crystallization usually occurred around 1150±50 K (the error includes the dispersion among the various samples). For the samples in the BN matrix instead, exceptional supercooling rates down to 900±50 K were found. This is a clear indication that a certain form of interaction between Ge particles and inert matrix occurs. The experimental findings suggest that graphite particles are wetted by liquid Ge and are able to stimulate crystallization of the Ge droplets whereas BN particles are less effective in this respect.

After the experiment, the recrystallized sample can be cooled down to room temperature in vacuum and the spectrum compared with the known c-Ge spectrum. This comparison for both Ge in BN and graphite matrices confirms the identity of the sample nature before and after prolonged high-temperature exposition.

E. XAS measurements

Measurements of purified c-Ge have been recorded at 77, 297, 450, 620, 780, 920, and 1100 K. The temperature error is indicated in Table I. The a-Ge sample was measured at room temperature only. Examples of raw absorption data for c-Ge and a-Ge are reported in Fig. 4.

The c-Ge EXAFS signals weighted by k^2 are reported in Fig. 5. The quality of the measurements is very good as can be observed.

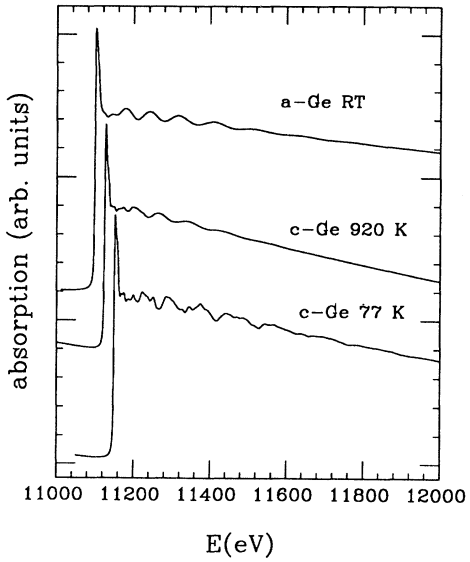

FIG. 4. Raw x-ray-absorption spectra for c-Ge at 77 and 920 K, and for a-Ge at RT. The energy scales for the c-Ge spectra are shifted by 25 and 50 eV, respectively. The absence of any feature associated with oxide contamination is evident.

Measurements of molten Ge have been performed covering a wide range of temperatures from highly supercooled liquid conditions at 950 K to the hot liquid just below the evaporation threshold around 1610 K. The complete list of measurements with indication of the sample matrix is reported in Table II.

The raw $k\chi(k)$ data for the liquid Ge are reported in Fig. 6, for the various temperatures, as well as the previous c-Ge spectrum at 1100 K for comparison. The dramatic differences of the EXAFS between c-Ge and l-Ge are evident; they are a direct manifestation of the increased width of the first-shell peak and increased average distance. There is also a remarkable trend in the intensity and profile of the l-Ge spectra on increasing temperature. This trend is evidenced in Fig. 7 where three significant spectra are compared on the same base line. A clear phase shift and amplitude reduction of about 50% are observed from 950 to 1610 K.

TABLE I. Summary of the structural results for the first-shell bond length distribution in c-Ge as a function of temperature and comparison with a-Ge at RT.

T (K)	ρ (Å^{-3})	$a_0\sqrt{3}/4$ (Å)	R (Å)	σ^2 (Å^2)	β
77(+10)	0.04431	2.4474	2.449(2)	0.0023(2)	0. (f)
297(2)	0.04418	2.4498	2.449(2)	0.0036(1)	0. (f)
450(10)	0.04406	2.4520	2.451(2)	0.0048(1)	0.00(10)
620(20)	0.04391	2.4548	2.456(2)	0.0067(1)	0.10(10)
780(20)	0.04377	2.4573	2.460(3)	0.0087(2)	0.15(10)
920(20)	0.04363	2.4600	2.462(3)	0.0102(2)	0.16(10)
1100(20)	0.04345	2.4634	2.466(3)	0.0130(2)	0.16(10)
a-Ge at 297 K	$N = 3.9(1)$				
297(2) K	0.044	–	2.464(2)	0.0054(1)	0.21(10)

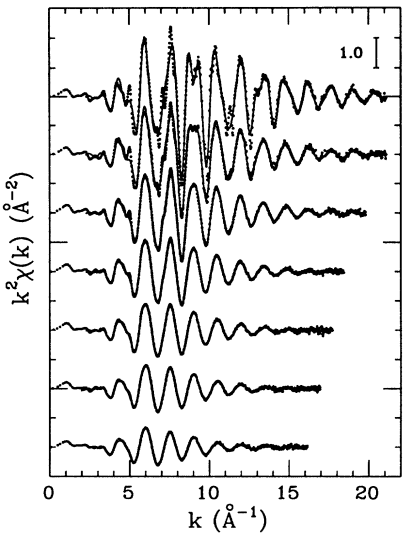

FIG. 5. EXAFS spectra of c-Ge as a function of temperature. From top to bottom the nominal temperatures in K are 77, 297, 450, 620, 780, 920, and 1100, respectively. The effect of the thermal vibrations is evident. The solid lines interpolating the data points are the best fits with theoretical signals including contributions up to the third-shell frequency.

The quality of the measurements is excellent; the noise, visible due to the amplified scale of the plot, is always in the 10^{-4} range of the absorption scale. The l-Ge $\chi(k)$ signal is minuscule, never exceeding 0.006 units; nevertheless, our measurements are able to detect signal up to 10–12 Å^{-1}. This is of extreme importance to get a correct distance determination. By comparison these maximum k values are equivalent to $k \approx 20$ Å^{-1} in a diffraction experiment, which is often not even reached by those measurements. This clearly demonstrates the power of the EXAFS technique and the existence of a completely open research field in which EXAFS can be successfully applied.

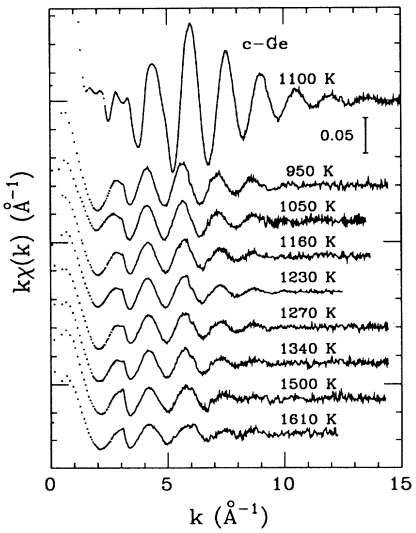

FIG. 6. Experimental $k\chi(k)$ spectra for l-Ge measured at the following temperatures in K: 950, 1050, 1160, 1230, 1270, 1340, 1500, and 1610. The top spectrum is c-Ge at 1100 K reported on the same scale for comparison.

TABLE II. XAS measurements on liquid Ge; the first three temperatures correspond to supercooled liquid samples. In the second column BN indicates a boron nitride matrix, C a graphite matrix. For each measurement the maximum EXAFS k value (k_{max}) is reported. The maximum value of the $g(r)$ (g_{max}) and the r value where $g(r) = 0.5$ ($r_{0.5}$) are also reported, according to our analysis.

T(K)	Matrix	k_{max} (Å^{-1})	g_{max}	$r_{0.5}$ (Å)
950(20)	BN	14.5	2.30(5)	2.340(10)
1050(10)	BN	13.5	2.20(5)	2.330(10)
1160(10)	C	13.5	2.01(5)	2.315(10)
1230(10)	C	12.5	2.01(5)	2.310(10)
1270(30)	C	14.5	1.97(5)	2.290(10)
1340(30)	C	14.5	2.00(5)	2.280(10)
1500(50)	C	14.5	1.95(5)	2.270(10)
1610(60)	C	12.5	1.83(5)	2.260(10)

III. DATA ANALYSIS AND RESULTS

Data analysis has been performed using the GNXAS package.[29–31] Phase shifts for photoabsorber and backscatterer atoms have been calculated for the c-Ge configuration using tangent muffin-tin spheres. Single-scattering and MS signals were calculated for the most important configurations required for the analysis of the various Ge specimens. Fitting was performed directly on the absorption data without any noise filtering or preliminary background subtraction. Statistical error analysis

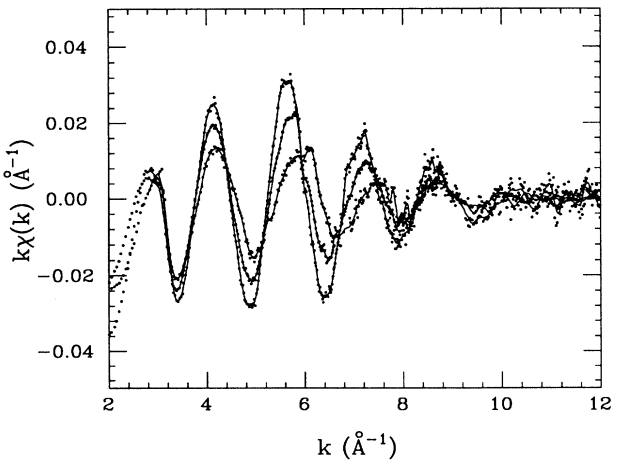

FIG. 7. Comparison of the experimental $k\chi(k)$ spectra for l-Ge at 950, 1230, and 1610 K on the same base line. There is an evident trend in the amplitude and a slight shift in the phase.

has been performed using standard criteria.[31]

Empirical parameters have been calibrated on the room-temperature c-Ge spectrum. In particular the overall amplitude reduction factor S_0^2 was found to be 0.90(3) and has been fixed to 0.9 in the present analysis. The position for the zero of the theoretical energy scale was found to be (in our energy calibration) $E_0 = 11107.6$ eV, corresponding to the vertical arrow in Fig. 3. With this calibration a very accurate relative comparison can be performed among the various spectra. The transferability of these values to different condensed phases of Ge is very high and is not a source of systematic errors.

A. Double-electron excitation

The importance of accounting for double-electron excitation effects in the atomic background, especially in the case of highly disordered solids or liquids, where the structural signal is intrinsically weak, has been widely emphasized elsewhere.[53]

Heavy fourth-period atoms are known to be affected by double-electron excitations of the $1s$ and either $3d$ or $3p$ electrons to unoccupied states. These transitions have been widely studied in Kr (Ref. 54) and Br (Ref. 55), but are clearly present also in lighter elements (as, for example, in the Ga case[34]). In Ge the additional binding energy of the $3d$ and $3p$ electrons in the presence of a $1s$ hole can be estimated looking at the binding energies for the As atom. These are ≈ 42 and ≈ 142 eV, respectively.

In Fig. 8 raw absorption spectra of Ge samples are reported after the subtraction of an average linear decay. In this way the fine structure can be magnified without adding any spurious curvature. The upper spectrum is the raw absorption of l-Ge at 1230 K; the lower one is for c-Ge at 1100 K. In both cases the expected structural signal is a regular damped sinusoidal oscillation. Instead, it is clear that both spectra present evident anomalies. The first one is the relatively sudden rise of the whole spectrum base line around 11 150 eV. This is a typical feature for Ge K-edge spectra and usually the EXAFS analysis is performed beyond this point. The second feature, mainly visible in l-Ge, is a doubly peaked relatively low second maximum of the fine structure (magnified inset in Fig. 8). While the full analysis of the EXAFS oscillation will be reported below, it can be anticipated that after suppression of the stronger first-shell contribution the same feature becomes visible in the c-Ge spectrum. Both features are clearly associated with an underlying double-step background quite similar to the one observed in HBr.[55,53] In particular the dip in the second maximum of the l-Ge EXAFS is associated with the onset of the $[1s3p]$ channels.

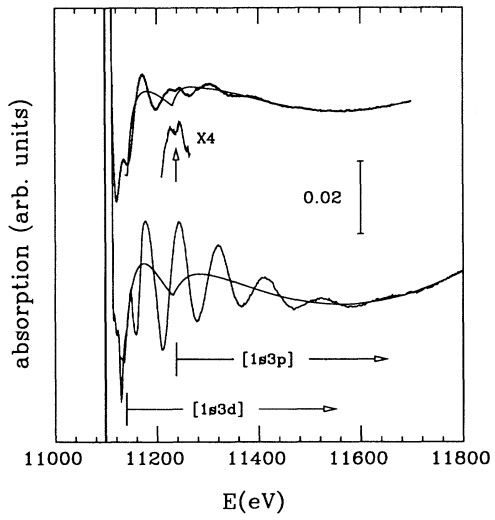

FIG. 8. Magnified absorption spectra for l-Ge at 1230 K and c-Ge at 1100 K. In both spectra the rise of the absorption associated with the onset of $[1s3d]$ channels, around 11 140 eV, is evident. A weaker feature is clearly visible in the l-Ge spectrum around 11240 eV, magnified in the inset, that is associated with the onset of $[1s3p]$ channels. Both effects can be accounted for using an empirical background model reported as a thin solid line on the corresponding base lines for c-Ge and l-Ge spectra.

Following previous guidelines and criteria, well established within the GNXAS methodology,[29] we modeled the atomic background introducing two steps accounting for the two double excitations, using widely tested empirical models.[56] The model background optimized on the the l-Ge and c-Ge spectra are the smooth curves with two rounded steps reported in Fig. 8 on the corresponding base lines. This nonstructural background is real and is not an artifact of the analysis; the shape is consistent with the shape of the same excitations in bromine,[55,53] and the energies are consistent with the $Z+1$ onset estimates. The only adjustable parameter is, in practice, the intensity that in this case turns out to be reasonable in terms of previous findings.

The present model background may introduce some uncertainty in the region of the two cusps, around 3.0 Å^{-1} and 6.0 Å^{-1}, due to the possible presence of resonance peaks that are not accounted for; however, it certainly reproduces the main behavior of the shakeup and shakeoff contributions. Apart from the two narrow double-excitation threshold regions, the empirical background model does not add any spurious high-frequency component to the spectrum.

As apparent from Fig. 8 an account for the double-electron excitation background is essential for the interpretation of the l-Ge spectra and strongly recommended for the high-temperature c-Ge spectra, but certainly less important for the analysis of the room-temperature data. This explains why in all of the previous investigations these features have been neglected. When high-temperature spectra are taken or when data are compared with theoretical model signals, their inclusion is, however, necessary. The fact that the double-excitation background generates a fine structure of comparable intensity with the structural contribution does not prevent us from performing an accurate EXAFS analysis. The developments of advanced methods for EXAFS data analysis, like the GNXAS approach, already enabled us to tackle a wide range of complex structural problems.

B. c-Ge data analysis

The analysis of the c-Ge data has been carried out accounting for the first, second, and third coordination shells. The first-shell analysis can be carried out in an independent manner and within the single-scattering approximation. The analysis of the successive shells instead requires the inclusion of MS effects. The importance of MS signals associated with the basic triangle occurring in the diamond coordination was first revealed in c-Si (Ref. 57) and a-Si (Ref. 58). Similarly MS is found to be important to describe correctly the signal in the second-shell frequency region of c-Ge. The complete analysis for the room-temperature c-Ge spectrum up to the third shell including MS effects has been described in detail elsewhere.[31,46] In this paper we will limit the presentation to the first coordination shell results as a function of temperature.

The best fits of the c-Ge data were shown in k space in Fig. 5 as the solid lines interpolating the data-point spectrum. The magnitudes of the Fourier transforms (FT's) in the first-shell distance region are reported in Fig. 9. As usual the fits are performed directly on the raw data without any noise filtering and the k and R space diagrams represent only a convenient way to report the results. The quality of the fits is excellent.

The RT a-Ge spectrum was also fitted with similar criteria. In this case the signal is dominated by the first-shell component. The single-shell fit in k and R space is reported in Fig. 10.

In the GNXAS methodology full account for the curved wave effects in the configurational average is taken. This

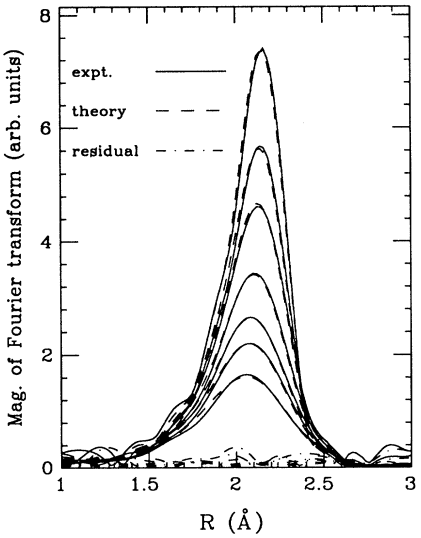

FIG. 9. Magnitude of the Fourier transforms of the c-Ge EXAFS spectra of Fig. 5, in the first-shell region, compared with the same quantities calculated for the fitting theoretical signals (dashed lines). The Fourier transforms of the residual signals are also reported (dot-dashed curves). The R values are not corrected for the phase shift and therefore do not correspond to a physical distance.

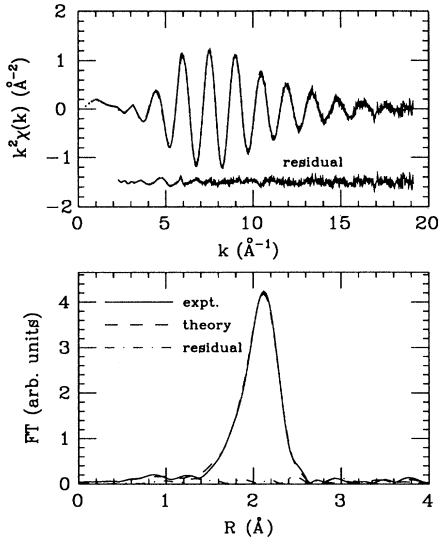

FIG. 10. Fit of the RT a-Ge spectrum comparison between experimental spectrum and calculated first-shell signal in k (upper plot) and R (lower plot) spaces. The residual difference spectrum and its Fourier transform are also shown.

is obtained using a numerical procedure in the signal computation[59,30] that is equivalent to more involved analytical methods.[60] In the present case a second-order Taylor expansion for amplitude and phase has been used. A clear separation is maintained between signal shapes and geometrical parameters, so that the latter can be directly obtained from the fitting procedure and do not require any correction for spurious effects (like mean free path, etc.).

The structural parameters have been determined by the least-squares conditions and the correlated statistical errors evaluated by means of a full statistical analysis.[31]

C. c-Ge (a-Ge) results

The structural results for the first-shell c-Ge data as a function of temperature and for the a-Ge RT spectrum are reported in Table I.

The bond length probability density $p(r)$ was modeled using a Γ-like distribution. Its general expression,[61] valid for $(r-R)\beta > -2\sigma$,

$$p(r) = \frac{2}{\sigma|\beta|\Gamma(\frac{4}{\beta^2})}\left(\frac{4}{\beta^2}+\frac{2(r-R)}{\sigma\beta}\right)^{\frac{4}{\beta^2}-1} \times \exp\left[-\left(\frac{4}{\beta^2}+\frac{2(r-R)}{\sigma\beta}\right)\right] \quad (1)$$

depends on three parameters: the average distance R, the variance σ^2, and the adimensional skewness parameter $\beta = K_3/\sigma^3$, where K_3 is the third cumulant of the distribution. $\Gamma(p)$ is the Euler's gamma function and is calculated for $p = 4/\beta^2$ defined on the positive real axis.

The $p(r)$ describes the probability density of finding a

bond with distance r and its shape can be varied continuously from positive to negative asymmetry through the Gaussian limit $\beta = 0$. The EXAFS signal is averaged over $p(r)$ and is multiplied by the coordination number parameter N. N was fixed to 4 for c-Ge and floated around 4 for a-Ge. If N is floated, the asymmetric model depends on a total of four parameters. The peak profile in the radial distribution function $g(r)$ scale is given by

$$g(r) = \frac{Np(r)}{4\pi\rho r^2}. \tag{2}$$

Strictly speaking the profile shapes are not the same in the two representations; EXAFS measures the $Np(r)$ function and our parameters refer to that one. In order to calculate the $g(r)$ an external input of the density ρ of the material is required.

Other authors have interpreted the c-Ge (and a-Ge) EXAFS spectra in terms of the cumulant expansion method.[42] This method is based on a power-law fitting of the logarithm of amplitude ratio and of the phase difference with respect to a reference spectrum, possibly recorded at low temperature. Usually, estimates for the third K_3 and fourth K_4 cumulants of the bond distribution can be obtained. This procedure can be used only for small deviations from Gaussianity; otherwise, it is likely that the fitted functions actually depend on a larger number of K_n coefficients or, even, that the cumulant expansion is not convergent at all.

We believe that there are some advantages using our procedure even if it is model dependent. We point out that the knowledge of the first four cumulants does not allow one to retrieve the distribution shape; for instance, no distribution exists with $K_3 \neq 0$ and $K_4 \neq 0$ but $K_{n>4} = 0$, because the integral inverse Fourier transform of the characteristic function would become negative in some regions or even is not convergent at all if $K_4 > 0$. Moreover, for small deviations from the Gaussian limit the K_4 parameter is estimated with a large statistical error.

In Table I the successive columns report the sample temperature, the corresponding c-Ge density and crystallographic average bond length $a_0\sqrt{3}/4$ (a_0 being the cubic cell size) obtained from thermal expansion data[62] and the room-temperature lattice parameter,[63] and finally the EXAFS average bond length R, the variance σ^2, and skewness β parameters.

The evident expansion of the average bond length is reported in Fig. 11. The solid line refers to $a_0\sqrt{3}/4$, and is compared with the experimental determination of R. Strictly speaking R and $a_0\sqrt{3}/4$ are different quantities, the former being also sensitive to the positive contributions from the perpendicular vibrations. This effect has been previously discussed in an EXAFS investigation of β-AgI.[64] To lowest order R is approximately given by

$$R \sim a_0\sqrt{3}/4 + \frac{\sigma_\perp^2}{R}, \tag{3}$$

where $\sigma_\perp^2 = \langle[(\mathbf{r_i}-\mathbf{r_j})\cdot\hat{v}_\perp]^2\rangle$ is the vibrational variance of the instantaneous first-neighbor distance projected along any direction $\hat{v}_\perp$ orthogonal to the bond average direction. The difference of 0.004 Å at 1100 K can be obtained with $\sigma_\perp^2 \sim 0.01$ Å^2 which is a reasonable value.

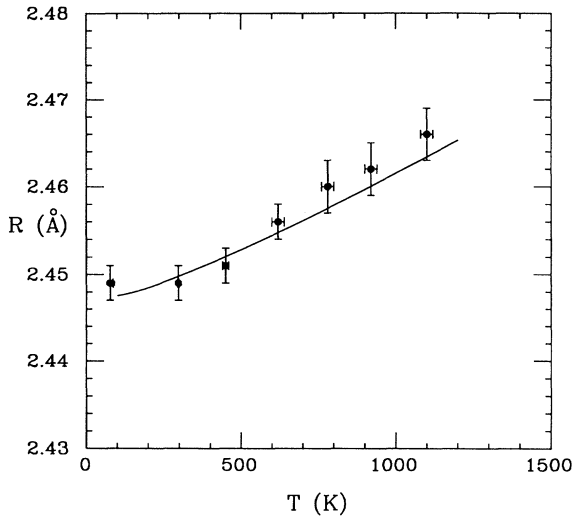

FIG. 11. Average of the first-shell bond length for c-Ge, as a function of temperature, compared with the average crystallographic bond length (solid line). The slightly higher expansion in the EXAFS parameter is due to the effect of the vibrations orthogonal to the bond direction.

The temperature variation of the variance of the bond length distribution σ^2 is reported in Fig. 12. Our measurements are found to be in excellent agreement with the pioneering EXAFS experiment by Crozier and Seary.[38] Our experimental points are found to be in very good agreement also with previous calculations performed in the harmonic approximation using the bond-charge model[65] or a Keating potential adjusted on the

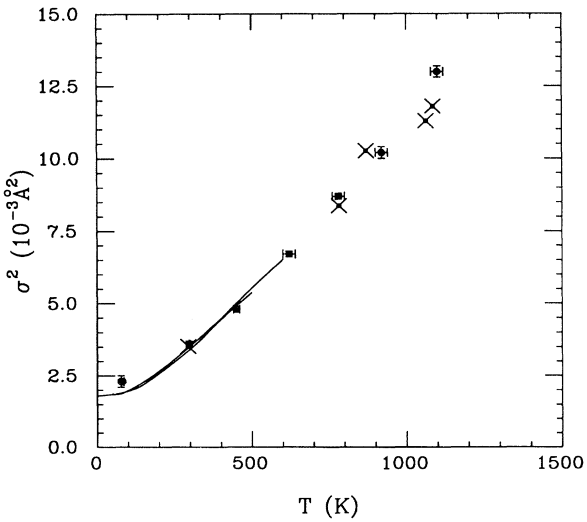

FIG. 12. Variance of the bond length distribution in c-Ge from the EXAFS data (points) compared with the calculations of harmonic force models (solid line) and previous data (Ref. 38) (× symbols).

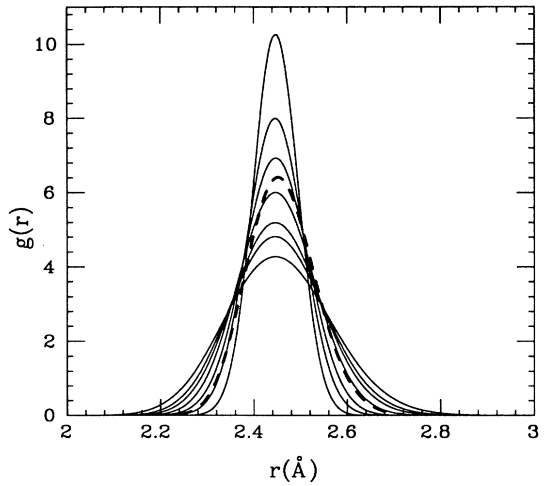

FIG. 13. First-shell $g(r)$ peak profiles of c-Ge at the same temperatures as in Fig. 5 compared with the a-Ge RT data (dashed line) as determined by the present analysis.

second and fourth moments of the vibrational density of states.[66] The σ^2 of the first-shell of c-Ge closely follows a harmonic behavior and very little deviations from the high-temperature linear classical limit are found.

The temperature dependence of the skewness parameter β is reported in Table I. In line with previous results,[38] only a little asymmetry is measured at high temperature. Due to the small values of β the assumptions on the peak profile are not a limiting factor in our analysis.

The results for a-Ge at RT, reported on the bottom line of Table I, are consistent with previous EXAFS and diffraction investigations.

From the values of R, σ^2, and β, the Γ model distribution, and the calculated densities reported in Table I, peak profiles for the first-shell distribution in c-Ge at various temperatures have been calculated. The profiles in the $g(r)$ scale [Eq. (2)] for the various temperatures are compared in Fig. 13. The progressive broadening and the onset of the asymmetry are apparent. For comparison the a-Ge peak profile at RT is also reported as a dashed curve. The density in this case was assumed to be 0.044 $Å^{-3}$. The peak reaches the height of 6.4 and the parameters are in perfect agreement with previous neutron-diffraction data.[67]

These results epitomize the sensitivity of the EXAFS technique to the first-shell peak profile and even to very small variations in its shape and position. A main advantage of the EXAFS is that the same physical quantity can be measured and compared between crystalline and disordered specimens.

D. l-Ge data analysis

The difficulties in interpreting EXAFS data from liquid systems have been widely emphasized in the literature, the problem mainly arises from the strong asymmetry of the first $g(r)$ peak that continuously merges into the long distance tail. Although not directly affecting the EXAFS signal the tail prevents one from performing a single-shell fitting in a consistent way. In a previous investigation on liquid lead[68] it was clearly shown that a standard EXAFS analysis yielded coordination numbers lower than those expected from the known $g(r)$. More recently the use of a careful analysis on EXAFS spectra of liquid and supercooled Ga (Ref. 35) allowed us to derive short-range $g(r)$ properties in good agreement with diffraction results and to detect MS effects associated with three-body configurations.

In our opinion the EXAFS data analysis cannot ignore the information on the $g(r)$ functions obtained from diffraction experiments. A method to analyze spectra of liquid systems combining previous long-range information on the $g(r)$, possibly from diffraction data or simulation, with the short-range sensitivity of the EXAFS has been described in a previous paper.[32] The method that is going to be used in the present investigation on l-Ge is able to provide refined $g(r)$ models directly comparable with previous experiments or computer simulations.

A preliminary insight into the interpretation of the EXAFS from liquid matter can be given by the calculation of the EXAFS associated with different $g(r)$ models. This can be done in a straightforward manner using the equation

$$\chi(k) = \int_0^\infty 4\pi r^2 \rho\, g_2(r)\, \gamma^{(2)}(r,k)\, dr, \qquad (4)$$

where the function $\gamma^{(2)}(r,k)$ is the EXAFS signal associated with the presence of a single atom at distance r from the photoabsorber. Previous applications of Eq. (4) can be found elsewhere.[61,32] In the Ge case, the few empirical parameters required to model the signal can be reliably calibrated on the c-Ge spectrum.

Using Eq. (4) we calculated several $\chi(k)$ signals associated with previously reported $g(r)$ data. The results are compared with the experimental spectrum at 1230 K on the $k\chi(k)$ scale in Fig. 14. We emphasize that due to the large short-range sensitivity of the EXAFS very subtle differences between the spectra may be amplified. Because of the poor resolution of the $g(r)$ distributions, especially on the first rise, the actual calculated spectra should be taken with caution. In any case the comparison indicates an excellent agreement of the experimental EXAFS with both calculated signals from the ND $g(r)$ by Salmon[28] and from *ab initio* MD $g(r)$ results by Kresse and Hafner.[20] While it is still early to make any evaluation of the present data, it is clear that XAS can provide fruitful information in understanding the short-range order in liquids, and that there is a wide complementarity between EXAFS and diffraction data.

Further progress in the understanding of the l-Ge EXAFS is obtained by the application of the peak fitting procedure to refine the short-range shape of a starting $g(r)$ model.[32] The method,[32] in practice, provides constraints on the coordination number parameters in the fitting procedure.

As a starting $g(r)$ model we used a smoothed version of the MD simulation results by Kresse and Hafner.[20] At a successive stage also different starting models will be used

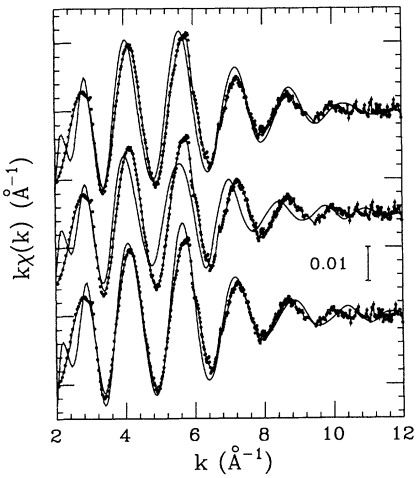

FIG. 14. Comparison between the experimental EXAFS spectra at 1230 K (dotted lines) and calculated $k\chi(k)$ signals for $g(r)$ functions previously reported in the literature (solid lines). Calculation from neutron diffraction $g(r)$ (Ref. 28) (top curve), calculation from recent energy-dispersive x-ray diffraction $g(r)$ (Ref. 24) (middle curve), calculation from *ab initio* MD simulation (Ref. 20) (bottom curve).

to investigate the effects on the final refined $g(r)$. The $g(r)$ was decomposed into a first asymmetric peak plus a long-distance tail. The tail contribution was calculated using Eq. (4) and kept fixed in the refinement. The peak contribution was instead fitted to the available EXAFS data, with a coordination number constraint, and only three free parameters. It has been demonstrated that this procedure guarantees that the compressibility limit $k \to 0$ of the structure factor $S(k)$ associated with the model $g(r)$ is not altered in the refinement.[32]

An optimized fit of the l-Ge signal at 1230 K is reported in Fig. 15. The difference residual spectrum is also reported for comparison. While the overall agreement is acceptable, there are several discrepancies in the low- and high-k regions well above the noise level. In the high-k region it is possible to observe a dephasing of the experimental oscillation with respect to the simulated one. Because of the freedom in the parameters, any asymmetric peak with a Γ distribution shape could have been generated. The discrepancy indicates that a more flexible model function is required. The next logical step is to allow the existence of two Γ-function components in the first-shell peak. By doing this, in addition to the coordination number constraint a further constraint on the second moment of the total two-peak distribution was imposed. It has been shown[32] that this corresponds to the requirement

$$\lim_{k\to 0} \frac{\partial^2 \Delta S(k)}{\partial k^2} = 0, \tag{5}$$

where $\Delta S(k)$ stands for the difference of the $S(k)$ between the original model and refinement. In practice this procedure is very effective in reducing the number of structural parameters. In this case the two peaks de-

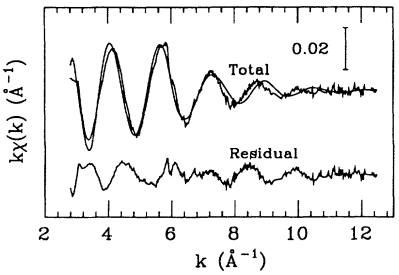

FIG. 15. Analysis of the 1230 K l-Ge $k\chi(k)$ spectrum using a model $g(r)$ made of a single Γ-distribution peak plus a tail contribution. The experimental signal is compared with the calculated total signal (solid curve). There is a clear mismatch in the amplitude and also in the phase, indicating that a more flexible first-peak profile is required. The bottom curve is the residual difference spectrum.

pend on a total of six parameters only. We point out that the constraint on the total coordination number of the two short-range peaks does not impose a real coordination number constraint on the first-neighbor distribution, since the second peak can distribute the excess atoms at larger distances in the tail region.

The best-fit analysis is reported in Fig. 16 where the partial first peak, second peak, and tail components are also shown. The interference between the two main signals is now able to reproduce the high-k region of the spectrum in a perfect manner. This excellent explanation of the phase behavior in the high-k region obtained with the two-peak fitting and the improvement with respect to the single-peak model indicates that there is enough

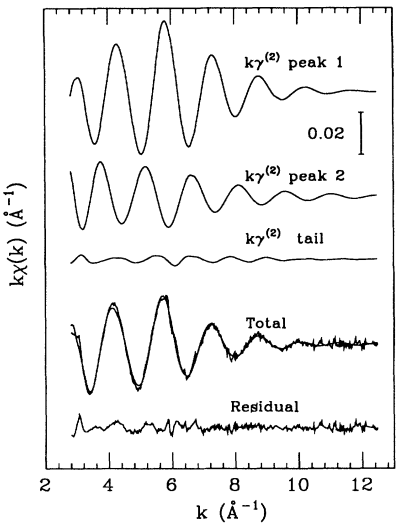

FIG. 16. Analysis of the 1230 K l-Ge $k\chi(k)$ spectrum using a model $g(r)$ composed of two Γ-distribution peaks plus a tail contribution. The $k\chi(k)$ signals associated with the three separate contributions are reported as well as the comparison between the experimental signal and the total theoretical signal and the residual, similarly to Fig. 15. The quality of the fit is significantly improved.

structural information in the $\chi(k)$ to fit six parameters to reproduce the signal associated with the short-range $g(r)$ shape.

E. *l*-Ge results

The information on the $g(r)$ of liquid Ge contained in the $\chi(k)$ is very valuable and the purpose of the present analysis is to understand the differences among the signals at the various temperatures as well as the overall oscillatory content. The entire set of data available for *l*-Ge was fitted with similar criteria [starting from the MD model $g(r)$]. The corresponding results on the $k\chi(k)$ scale are reported in Fig. 17. Similarly the magnitudes of the Fourier transforms for experiment, theory, and residual are reported in Fig. 18. The capability of the model to explain the observed signal in the whole temperature range is evident.

The fitting allowed us to derive refined short-range $g(r)$ functions at the various temperatures. In order to check the influence of the starting model and associated long-range tail on the final results and to assess the reliability of the method, the entire analysis was repeated using, as a starting model, the $g(r)$ obtained from the Salmon's ND measurement.[28] A compilation of the r space results is reported in Fig. 19. On each temperature base line the two solid curves refer to the EXAFS-optimized $g(r)$'s obtained from the two different initial models, and comparison is made with the ND data.[28] The two total refined $g(r)$'s differ slightly around 3.5 Å but are substantially indistinguishable in the first-peak region. This is a clear demonstration that the results obtained with the present method are largely independent of the initial model. For each $g(r)$ plot the profiles for the two Γ distributions and the tail components, obtained in the MD data refinement, are also reported.

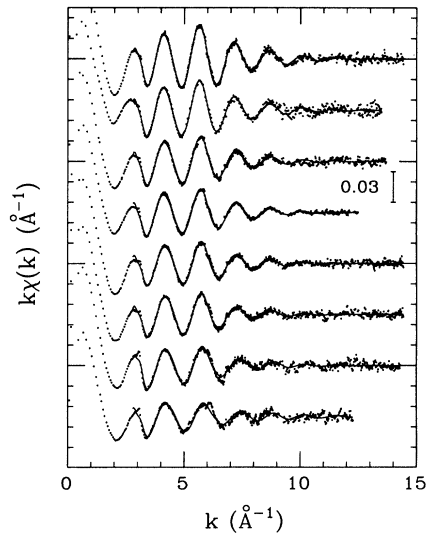

FIG. 17. Analysis of the structural oscillations in all of the available *l*-Ge spectra. The best-fit (solid line) $k\chi(k)$ functions for each experimental spectrum (dotted lines) are reported on the corresponding base lines. The spectra are shifted by 0.05 Å^{-1} on the ordinate scale for clarity.

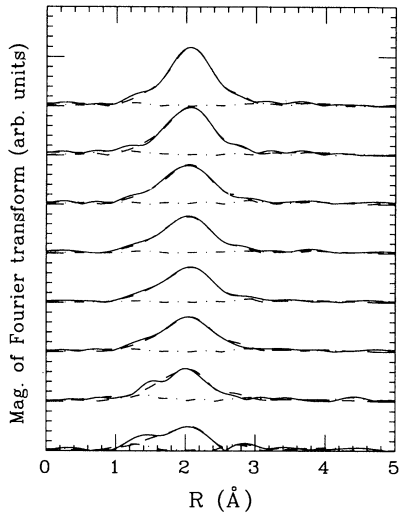

FIG. 18. Magnitudes of the Fourier transforms (FT's) of all of the available *l*-Ge spectra, calculated in the range 2.8–12.0 Å^{-1} with a k weight. For each temperature, the FT's of the experimental data (solid line), the FT's of the model signal (dashed line), and the FT's of the residual difference spectrum (dot-dashed line) are reported. On this scale the agreement between theory and experiment is excellent.

The interpretation of the two-peak model in terms of the appearance of the two coexisting populations of covalentlike and metalliclike bonds is very tempting. The two peaks account for about 1.8 and 5.0 atoms, respectively. However, since the two distributions strongly overlap, this separation is not based on any physical evidence. The double-peak model should be regarded just as a data-analysis device. Nevertheless, the requirement of a relatively structured model profile certainly reflects the complexity of the bonding nature in *l*-Ge.

A summary of the present measurements for *l*-Ge is reported in Table II. Since the signal coming from each component has no physical meaning, the numerical parameters for each shell are not reported. Instead physical meaning is contained in the total contribution that represents the refined $g(r)$ measured by EXAFS. The height of the maximum of the $g(r)$ and the distance for which the value $g(r) = 0.5$ is reached $r_{0.5}$ are reported in Table II. The uncertainty in the EXAFS parameters induces an uncertainty in the $g(r)$ shape, which is probably less than 0.05 units in the first-peak rise, maximum included, and increases to 0.1 units in the successive descent. In the tail region the uncertainty depends on the reliability of the original model but eventually the correct asymptotic behavior is guaranteed. The accuracy of the method in the first-peak region is demonstrated by the similarity of the refined $g(r)$ functions starting from different models. The advantages of our data analysis method[32] for disordered systems is that proper account is taken for the signal generated by the atoms in the intermediate-distance region corresponding to the first minimum of the $g(r)$. The only input from the original model is the $g(r)$ tail

profile and the $k \to 0$ properties of the $S(k)$ and its second derivative, which correspond to sum rules in r space. As a consequence the $g(r)$ profiles are realistic. This accuracy cannot be accomplished with other methods even based on the cumulant expansion technique.[69]

The strong short-range sensitivity of the EXAFS and the associated trend in the l-Ge spectrum as a function of temperature shown in Fig. 17 allowed us to perform a very accurate determination of the short-range properties of the $g(r)$. Some of the $g(r)$ functions reported in Fig. 19 are magnified and compared on the same scale in Fig. 20. As expected there is a clear regular trend in the $g(r)$ shape upon increasing temperature. The maximum of the $g(r)$ decreases from 2.30(5) in the supercooled liquid at 950 K, to about 2.00(5) in the liquid just above T_m, and down to 1.83(5) in the high-temperature liquid at 1610 K. These two latter values are in good agreement with the recent measurements by Petkov *et al.*,[24] and also with the neutron-diffraction result at 1273 K.[28] The comparison with the MD simulation[20] indicates that the actual $g(r)$ of the liquid at 1230 K is slightly lower than predicted, but there is a spectacular agreement in the peak position and rising edge. This comparison provides strong support to the validity of the present *ab initio* schemes and to the consistency of our results. Simultaneously to the peak-height decrease an overall broadening of the shape and a shift of the low-r edge towards shorter distances are observed. The latter is the direct manifestation in r space of the shift in the l-Ge $\chi(k)$ on increasing temperature. We estimate our sensitivity in the rising edge position to be 0.01 Å and in the maximum position to be 0.02 Å.

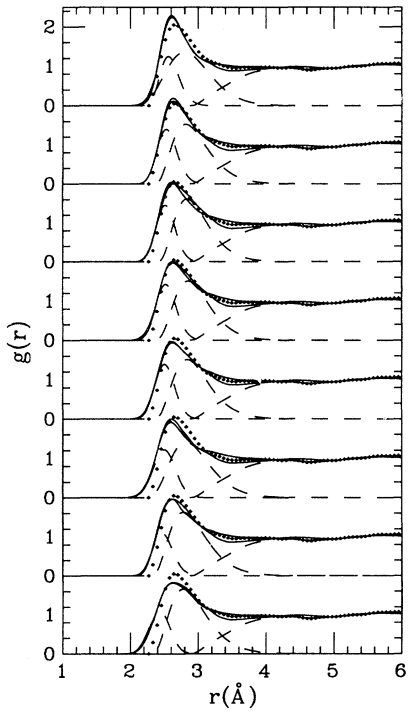

FIG. 19. Refined $g(r)$ models for l-Ge at the eight different temperatures. The offset between the curves is 2 units. For each temperature the two curves reported as solid lines refer to refinements obtained from different starting models. For comparison the $g(r)$ determined in the ND experiment at 1273 K (Ref. 28) is reported (dotted line). Typical $g(r)$ decompositions into three components (two fitted peaks plus the long distance tail) are also indicated (dashed curves). A significant trend in the shape of the first $g(r)$ peak is clearly revealed.

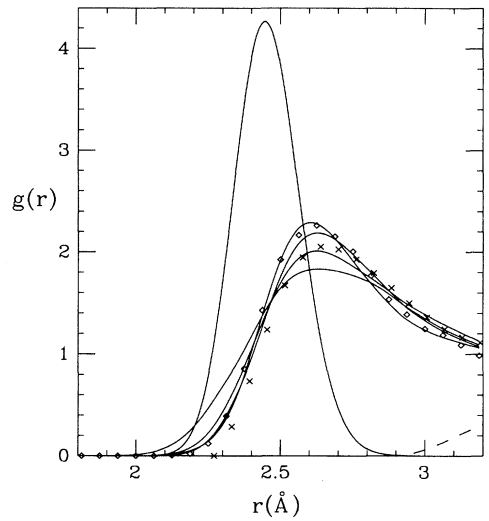

FIG. 20. Comparison between four refined refined $g(r)$ functions corresponding to 950, 1050, 1230, and 1610 K, representative of the whole set. The 950 K curve corresponds to the narrower and higher peak, the 1610 K one to the lower and broader peak. The positions of the maxima coincide within 0.02 Å and the differences should be mainly ascribed to the experimental uncertainty. The regular trend in the peak broadening and decrease of the minimum distance approach is instead significant. The MD result by Hafner and Kresse (Ref. 20) ($\diamond$) and ND data by Salmon (Ref. 28) ($\times$) are reported for comparison. The tail contribution fixed in the EXAFS refinement is also indicated (dashed line). The narrow peak with the maximum at 4.3 units is the first-shell c-Ge $g(r)$ peak at 1100 K reported for comparison.

The position of the maximum of the l-Ge $g(r)$, as derived from our EXAFS analysis, is found to be rather independent of the temperature resulting on the average 2.62(2) Å. This value as well as the position of the rising $g(r)$ edge are in excellent agreement with the *ab initio* MD results[20] and also with previous neutron-diffraction[28] data. Good agreement is also obtained with recent energy-dispersive x-ray-diffraction data.[24]

We believe that the accuracy of the EXAFS theory and the developments in the data-analysis procedures have come to a point in which the EXAFS technique is very reliable and the residual systematic errors are reduced below the statistical errors level,[31] also for the spectra of liquid systems. Thus, well-established diffraction techniques for studying liquid systems can nowadays be complemented by reliable EXAFS experiments characterized by a large short-range sensitivity.

EXAFS has also a certain number of experimental advantages over diffraction, in particular (1) the fast acqui-

sition time and the possibility to repeat the experiment several times, (2) the higher effective k range reachable with present experimental setups, (3) the possibility to perform the same experiment and data analysis on the same sample in the crystalline and liquid phases, and (4) the absence of any background contribution from the "container."

Disadvantages of EXAFS are connected with the complex background subtraction that, at present, cannot be calculated theoretically. However, in several cases, Ge included, the subtraction can be done using empirical shapes with accurate results and can be calibrated on spectra of model systems. The reliability of the present background subtraction scheme is also supported by the high quality of the fitting and the excellent agreement of the structural results with the known properties of l-Ge. Thus time is probably mature for a critical evaluation of the available structural data on l-Ge, to which the present EXAFS investigation can certainly give a large contribution.

The present results are based on EXAFS refinements involving only low-frequency components of the spectra. The residual spectrum, shown in Fig. 16, reveals the presence of a high-frequency component in the low-k region. This residual has an intensity comparable with the tail contribution, but certainly cannot be ascribed to errors in the evaluation of the signal associated with the $g(r)$. We anticipate here that attempts to include MS contributions associated with short-range three-body configurations were successful. In particular we were able to demonstrate the existence of a signal from equilateral triangular configurations among first neighbors. These configurations are characteristic of the close-packed metallic liquid structures and are associated with the principal feature of the triplet distribution function.

IV. CONCLUSION

A complete investigation has been carried out covering all ambient pressure phases of Ge in a wide temperature range from 77 to about 1600 K. Results have been also reported on metastable condensed states like a-Ge and, in particular, supercooled liquid Ge studied up to about 300 K below T_m. These latter measurements are of particular importance since they are the first available structural measurements on this nonequilibrium state. This achievement was possible by means of a newly developed technique for high-temperature XAS investigations[45] that allows one to study droplet samples well suited to reach supercooling conditions.[49]

The whole analysis has been carried out with the advanced GNXAS methodology and precise structural information has been obtained. The results are compared with theoretical calculations and simulations. Complete radial distribution functions were derived for the various cases.

Five main results represent an improvement with respect to previous investigations on these systems.

(1) The effect of two double-electron excitation channels has been clearly evidenced and included in the EXAFS data analysis.

(2) Structural parameters for the first-shell of c-Ge, in particular R, σ^2, and β, have been determined as a function of temperature from 77 to 1100 K. We point out that absolute σ^2 values can be derived from our analysis instead of differences with respect to model compounds.

(3) Structural measurements of supercooled liquid Ge were performed for the first time.

(4) EXAFS measurements for l-Ge are reported in a wide temperature range and a meaningful trend in the spectra and in the results was found. This represents a major advance with respect to the only previously attempted EXAFS experiment,[44] but also represents an amount of information comparable, if not bigger, than the whole set of existing diffraction experiments on l-Ge.

(5) The results on the $g(r)$ of l-Ge, and in particular the peak positions, are found in perfect agreement with previous neutron-diffraction determinations and with recent *ab initio* MD results.

All of the results reported in this paper clearly indicate that the potential of the EXAFS technique in probing the short-range order in highly disordered solids, or even liquid systems, is very high. The access to the extremely-high-temperature range[45] and the possibility to prepare stable liquid samples using recently developed techniques, together with advanced method for data analysis,[29–32] open a completely new field of investigation in the physics of condensed liquid matter. XAS is in fact nowadays able to provide quantitative information on the radial distribution function that can be directly compared with computer simulations or diffraction results. The strong complementarity between XAS and diffraction has been widely emphasized. As a result it appears advisable for future projects always to combine complex neutron-diffraction experiments with XAS experiments.

ACKNOWLEDGMENTS

Skillful operation of the DCI storage ring by the LURE staff is acknowledged. We are kindly grateful to Professor J. Hafner and to Dr. G. Kresse for sending us their original MD data and to Dr. P. S. Salmon for sending us his original neutron-diffraction $g(r)$ data. Thanks are due to Dr. J. P. Jtiè for stimulating discussions.

[1] J. C. Jamieson, Science **139**, 762 (1963).
[2] Y. K. Vohra, K. E. Brister, S. Desgreniers, A. L. Ruoff, K. J. Chang, and M. L. Cohen, Phys. Rev. Lett. **56**, 1944 (1986).
[3] F. P. Bundy and J. S. Kasper, Science **139**, 340 (1963); J. S. Kasper and S. M. Richards, Acta Crystallogr. **17**, 752 (1964).
[4] C. H. Bates, F. Dachille, and R. Roy, Science **147**, 860 (1965).
[5] R. J. Nelmes, M. I. McMahon, N. G. Wright, D. R. Allan, and J. S. Loveday, Phys. Rev. B **48**, 9883 (1993).
[6] A. Mujica and R. J. Needs, Phys. Rev. B **48**, 17 010 (1993).
[7] H. T. Hall, J. Phys. Chem. **59**, 1144 (1955).
[8] V. M. Glazov, S. N. Chizhevskaya, and N. N. Glagoleva,

Liquid Semiconductors (Plenum, New York, 1969).
[9] G. Devaud and D. Turnbull, Acta Metall. **35**, 765 (1987); in *Phase Transitions in Condensed Systems—Experiments and Theory*, edited by G. S. Cargill III, F. Spacepen, and K-N. Tu, MRS Symposia Proceedings No. 57 (Materials Research Society, Pittsburgh, 1987), p. 89.
[10] P. V. Evans, S. Vitta, R. G. Hamerton, A. L. Greer, and D. Turnbull, Acta Metall. **38**, 233 (1990); C. F. Lau and H. W. Kui, *ibid.* **39**, 323 (1991).
[11] G. A. N. Connell and R. A. Street, in *Handbook on Semiconductors*, edited by T. S. Moss and S. P. Keller (North-Holland, Amsterdam, 1980), Vol. 3.
[12] J. Hafner and G. Kahl, J. Phys. F **14**, 2259 (1984).
[13] N. W. Ashcroft, Nuovo Cimento D **12**, 597 (1990).
[14] K. J. Ding and H. C. Andersen, Phys. Rev. B **34**, 6987 (1986); W. D. Luedtke and U. Landman, *ibid.* **37**, 4656 (1988).
[15] A. Arnold, N. Mauser, and J. Hafner, J. Phys. Condens. Matter **1**, 965 (1989).
[16] R. Car and M. Parrinello, Phys. Rev. Lett. **55**, 2471 (1985).
[17] G. Kresse and J. Hafner, J. Non-Cryst. Solids **156**, 956 (1993).
[18] I. Štich, R. Car, and M. Parrinello, Phys. Rev. Lett. **63**, 2240 (1989); Phys. Rev. B **44**, 4262 (1991).
[19] G. Kresse and J. Hafner, Phys. Rev. B **47**, 558 (1993).
[20] G. Kresse and J. Hafner, Phys. Rev. B **49**, 14 251 (1994).
[21] N. Takeuchi and I. L. Garzón, Phys. Rev B **50**, 8342 (1994).
[22] B. R. Orton and S. P. Woodisse, J. Phys. F **3**, 1141 (1973).
[23] Y. Waseda and K. Suzuki, Z. Phys. B **20**, 339 (1975).
[24] V. Petkov, S. Takeda, Y. Waseda, and K. Sugiyama, J. Non-Cryst. Solids **168**, 97 (1994).
[25] J. P. Gabathuler and S. Steeb, Z. Naturforsch. A **34**, 1314 (1979).
[26] M. Davidovic, M. Stojic, and D. Jovic, J. Phys. C **16**, 2053 (1983).
[27] M. C. Bellissent-Funel and R. Bellissent, J. Non-Cryst. Solids **65**, 383 (1984).
[28] P. S. Salmon, J. Phys. F **18**, 2345 (1988).
[29] A. Filipponi, A. Di Cicco, T. A. Tyson, and C. R. Natoli, Solid State Commun. **78**, 265 (1991).
[30] A. Filipponi, A. Di Cicco, and C. R. Natoli (unpublished).
[31] A. Filipponi and A. Di Cicco (unpublished).
[32] A. Filipponi, J. Phys. Condens. Matter **6**, 8415 (1994).
[33] A. Filipponi, A. Di Cicco, M. Benfatto, and C. R. Natoli, Europhys. Lett. **13**, 319 (1990).
[34] A. Di Cicco and A. Filipponi, J. Non-Cryst. Solids **156-158**, 102 (1993).
[35] A. Di Cicco and A. Filipponi, Europhys. Lett. **27**, 407 (1994).
[36] A. Filipponi, P. D'Angelo, N. V. Pavel, and A. Di Cicco, Chem. Phys. Lett. **225**, 150 (1994).
[37] D. E. Sayers, E. A. Stern, and F. W. Lytle, Phys. Rev. Lett. **27**, 1204 (1971).
[38] E. D. Crozier and A. J. Seary, Can. J. Phys. **59**, 876 (1981).
[39] F. Evangelisti, M. G. Proietti, A. Balzarotti, F. Comin, L. Incoccia, and S. Mobilio, Solid State Commun. **37**, 413 (1981); F. Evangelisti, M. Garozzo, and G. Conte, J. Appl. Phys. **53**, 7390 (1982).
[40] E. A. Stern, C. E. Bouldin, B. von Roedern, and J. Azoulay, Phys. Rev. B **27**, 6557 (1983); M. A. Paesler, D. E. Sayers, R. Tsu, and J. Gonzalez-Hernandez, *ibid.* **28**, 4550 (1983); M. Wakagi, M. Chigasaki, and M. Nomura, J. Phys. Soc. Jpn. **56**, 1765 (1987); G. W. Johnson, D. E. Brodie, and E. D. Crozier, Can. J. Phys. **67**, 358 (1989); M. Wakagi and Y. Maeda, Phys. Rev. B **50**, 14 090 (1994).
[41] J. Freund, R. Ingalls, and E. D. Crozier, J. Phys. Chem. **94**, 1087 (1990).
[42] G. Dalba, P. Fornasini, M. Grazioli, and F. Rocca, J. Non-Cryst. Solids **164&166**, 159 (1993); (unpublished).
[43] G. Bunker, Nucl. Instrum. Methods **207**, 437 (1983).
[44] B. R. Orton, in *Neutron and X-ray Scattering*, edited by M. C. Fairbanks, A. N. North, and R. J. Newport, IOP Conf. Series No. 101 (Instute of Physics, Bristol, 1990), p. 77.
[45] A. Filipponi and A. Di Cicco, Nucl. Instrum. Methods B **93**, 302 (1994).
[46] L. Ottaviano, A. Filipponi, and A. Di Cicco, Physica B **208&209**, 337 (1995).
[47] J. Goulon, C. Goulon Ginet, R. Cortes, and M. Dubois, J. Phys. (Paris) **43**, 539 (1982).
[48] E. A. Stern and K. Kim, Phys. Rev. B **23**, 3781 (1981).
[49] L. Ottaviano, A. Filipponi, and A. Di Cicco, Phys. Rev. B **49**, 11 749 (1994).
[50] A. J. R. De Kock, in *Handbook on Semiconductors*, edited by T. S. Moss and S. P. Keller (North-Holland, Amsterdam, 1980), Vol. 3.
[51] D. Turnbull and R. E. Cech, J. Appl. Phys. **21**, 804 (1950); D. Turnbull, *ibid.* **21**, 1022 (1950).
[52] J. P. Itiè, J. M. Besson, A. Polian, D. Andrault, F. Farges, G. Fiquet, G. F. O. Graeff, and I. Chambuleyron (unpublished).
[53] A. Filipponi, Physica B **208&209**, 29 (1995).
[54] S. J. Schaphorst, A. F. Kodre, J. Ruscheinski, B. Crasemann, T. Åberg, J. Tulkki, M. H. Chen, Y. Azuma, and G. S. Brown, Phys. Rev. A **47**, 1953 (1993).
[55] P. D'Angelo, A. Di Cicco, A. Filipponi, and N. V. Pavel, Phys. Rev. A **47**, 2055 (1993).
[56] A. Filipponi, E. Bernieri, and S. Mobilio, Phys. Rev. B **38**, 3298 (1988).
[57] A. Di Cicco, A. Bianconi, and N. V. Pavel, Solid State Commun. **61**, 635 (1987); A. Bianconi, A. Di Cicco, N. V. Pavel, M. Benfatto, A. Marcelli, C. R. Natoli, P. Pianetta, and J. Woicik, Phys. Rev. B **36**, 6426 (1987).
[58] A. Filipponi, F. Evangelisti, M. Benfatto, S. Mobilio, and C. R. Natoli, Phys. Rev. B **40**, 9636 (1989).
[59] M. Benfatto, C. R. Natoli, and A. Filipponi, Phys. Rev. B **40**, 9626 (1989).
[60] C. Brouder, J. Phys. C **21**, 5075 (1988); C. Brouder and J. Goulon, Physica B **158**, 351 (1989).
[61] P. D'Angelo, A. Di Nola, A. Filipponi, N. V. Pavel, and D. Roccatano, J. Chem. Phys. **100**, 985 (1994).
[62] Y. S. Touloukian, R. K. Kirby, R. E. Taylor, and P. D. Desai, in *Thermophysical Properties of Matter*, edited by Y. S. Touloukian and C. Y. Ho (Plenum, New York, 1975), Vol. 12.
[63] J. F. C. Baker and M. Hart, Acta Crystallogr. **31a**, 2297 (1975).
[64] G. Dalba, P. Fornasini, R. Gotter, and F. Rocca, Phys. Rev. B (to be published).
[65] O. H. Nielsen and W. Weber, J. Phys. C **13**, 2449 (1980).
[66] A. Filipponi, Phys. Rev. B **37**, 7027 (1988).
[67] G. Etherington, A. C. Wright, J. T. Wenzel, J. C. Dore, J. H. Clarke, and R. N. Sinclair, J. Non-Cryst. Solids **48**, 265 (1982).
[68] E. A. Stern, P. Līviņš, and Z. Zhang, Phys. Rev. B **43**, 8850 (1991).
[69] E. A. Stern, Y. Ma, and O. Hanske-Petitpierre, Phys. Rev. B **46**, 687 (1992).